Nuclear Atrophy of Retinal Ganglion Cells Precedes the *Bax*-Dependent Stage of Apoptosis

Katherine T. Janssen,[1,2] *Caitlin E. Mac Nair,*[1,3] *Joel A. Dietz,*[1] *Cassandra L. Schlamp,*[1] *and Robert W. Nickells*[1]

Purpose. Retinal ganglion cells atrophy during the execution of the intrinsic apoptotic program. This process, which has been termed the apoptotic volume decrease (AVD) in other cell types, has not been well-characterized in ganglion cells.

Methods. Acute optic nerve crush was used to examine neuronal atrophy in the ganglion cell layer in wild-type and *Bax*-deficient mice. Nuclear size was measured from retinal wholemounts. Heterochromatin formation was assessed using transmission electron microscopy, whereas histone H4 acetylation was monitored using immunofluoresence. Ganglion cell and retinal transcript abundance was measured using quantitative PCR.

Results. Nuclear and soma sizes linearly correlated in both control and damaged retinas. Cells in wild-type mice exhibited nuclear atrophy within 1 day after optic nerve damage. Three days after crush, nuclear atrophy was restricted to ganglion cells identified by retrograde labeling, while amacrine cells also exhibited some atrophy by 5 days. Similar kinetics of nuclear atrophy were observed in cells deficient for the essential proapoptotic gene *Bax*. *Bax*-deficient cells also exhibited other nuclear changes common in wild-type cells, including the deacetylation of histones, formation of heterochromatin, and the silencing of ganglion cell–specific gene expression.

Conclusions. Retinal ganglion cell somas and nuclei undergo the AVD in response to optic nerve damage. Atrophy is rapid and precedes the *Bax*-dependent committed step of the intrinsic apoptotic pathway. (*Invest Ophthalmol Vis Sci.* 2013;54:1805–1815) DOI:10.1167/iovs.11-9310

From the [1]Department of Ophthalmology and Visual Sciences, University of Wisconsin, Madison, Wisconsin; [2]School of Medicine, University of Minnesota, Minneapolis, Minnesota; and the [3]Department of Pathology and Laboratory Medicine, University of Wisconsin, Madison, Wisconsin.

Supported by grants from the National Eye Institute (R01 EY012223 and R01 EY018869 [RWN] and P30 EY016665 vision science CORE grant to the Department of Ophthalmology and Visual Sciences, University of Wisconsin, Madison, Wisconsin), an American Health Assistance Foundation NGR grant (RWN), and unrestricted funding from Research to Prevent Blindness, Inc., to the Department of Ophthalmology and Visual Sciences, University of Wisconsin, Madison, Wisconsin.

Submitted for publication December 13, 2011; revised January 31, 2012 and January 18, 2013; accepted February 8, 2013.

Disclosure: **K.T. Janssen**, None; **C.E. Mac Nair**, None; **J.A. Dietz**, None; **C.L. Schlamp**, None; **R.W. Nickells**, None

Corresponding author: Robert W. Nickells, Department of Ophthalmology and Visual Sciences, University of Wisconsin, 6640 Medical Sciences Center, 1300 University Avenue, Madison, WI 53706; nickells@wisc.edu.

Retinal ganglion cells are long projection neurons of the central nervous system. The intrinsic apoptotic death of these cells is the primary feature of blinding optic neuropathies, of which glaucoma is the most common.[1,2] In glaucoma, the pathology that leads to ganglion cell death is still under considerable study. An elevation in IOP is the principal risk factor for the disease, and stress introduced by an increase in IOP is focused onto the optic nerve head where ganglion cell axons exit the eye. This is believed to alter glial behavior in the optic nerve head,[3–6] eventually leading to axonal damage, the loss of retrograde and anterograde transport, and the activation of axonal degeneration. A feature of ganglion cell death may be that it is compartmentalized, with the synapse, axon, dendritic arbor, and soma acting as autonomous, albeit linked, units that are affected in the dying cell.[7,8] Genetic manipulations in mice have clearly demonstrated that these compartmentalized degenerations are autonomous, and can occur even if one compartment has been prevented from degenerating.[7,9–11] From a viewpoint of therapeutic intervention of ganglion cell death, this sequential and potentially overlapping series of self-destruct pathways may represent windows of opportunity to rescue either the axon or soma, or both, of these cells.

Unlike necrosis, which is often characterized by an increase in cell volume,[12] apoptosis is associated with the shrinkage of cells. The early description of apoptosis remarked that cell atrophy, characterized by cell body and nuclear condensation, was a hallmark of cells dying by this process.[13] Others have attributed condensation, principally nuclear condensation, to occur in concert with fragmentation, the latter of which is dependent on the activation of caspases.[14,15] This places nuclear shrinkage as a late-stage event in the apoptotic series.

More recently, however, atrophy and shrinkage have been described as early events in apoptotic neurons, associated with changes in ion gradients across the plasma membrane.[16–18] This phenomenon has been termed the apoptotic volume decrease (AVD) and has typically reflected changes in total cell volume. Many dying neurons execute the AVD by invoking a rapid efflux of K^+ ions through delayed rectifier Kv-type potassium channels.[19] Principally, evidence suggests that phosphorylation and activity of the Kv2.1 channel is associated with neuronal apoptosis.[20,21] The placement of the AVD in the series of apoptotic events is still not clear, however, and may be composed of an early phase and a late phase.[22]

Ganglion cell atrophy has been described in several models of experimental glaucoma and acute optic nerve damage, in different species ranging from mice to cats to monkeys.[23–25] Detailed observations by Weber and colleagues,[23] in a nonhuman primate model of ocular hypertension, revealed a collapse and shrinkage of the dendritic arbor of individually labeled ganglion cells. In some neurons, the change in arbor area exceeded 40% of normal cells of the same class. Associated with the decrease in the dendritic arbor, retinal ganglion cell somas also exhibited upward of a 40% decrease in volume. Similar changes in the morphometry of cat retinal

ganglion cells were also observed in a cat model of acute optic nerve damage, changes that could be prevented by the immediate application of brain-derived neurotrophic factor (BDNF) by intravitreal injection.[24,26] More recently, using longitudinal imaging of retinal ganglion cells expressing Yellow Fluorescent Protein, Leung and colleagues[27] described a similar collapse of the dendritic tree of mouse retinal ganglion cells after optic nerve crush.

Here, we report quantitative studies to examine the kinetics of retinal ganglion cell atrophy in the mouse optic nerve crush model. In mice, ganglion cell layer neuronal soma size and nuclear size were directly proportional, even in damaged retinas, suggesting that nuclear atrophy occurred synchronously with soma atrophy. Nuclear shrinkage occurred within 24 hours after optic nerve damage and steadily progressed for at least 5 days after injury. Nuclear shrinkage also occurred in *Bax*$^{-/-}$ cells, which are blocked from completing the apoptotic program, indicating that this phenomenon is likely an early apoptotic response in ganglion cells. Additionally, other elements of nuclear changes, including widespread histone deacetylation, chromatin condensation, and the silencing of healthy ganglion cell gene expression, occurred in both wild-type and *Bax*-deficient ganglion cells, indicating that these changes are similarly an early event in the ganglion cell atrophy process.

Materials and Methods

Handling of Animals and the Optic Nerve Crush Protocol

Adult mice (3–6 months of age) were used for this study and handled in accordance with the Association for Research in Vision and Ophthalmology statement for the use of animals in research. All experimental protocols were approved by the Animal Care and Use Committee of the University of Wisconsin. *Bax*-deficient mice were generated from breeding of *Bax*$^{+/-}$ animals on a C57BL/6J genetic background. Cholinergic amacrine cells in the ganglion cell layer were genetically labeled by crossing *Rosa26R-LoxP-tdTomato* reporter mice with a transgenic line expressing Cre recombinase under control of the choline acetyltransferase (*Tg(Chat-cre)GM24Gsat*). These mice were a gift from Miles Epstein at the University of Wisconsin. Mice were housed in microisolator cages and kept on a 12-hour light/dark cycle and maintained on a 4% fat diet (8604 M/R; Harland Teklad, Madison, WI).

Optic nerve crush surgery was performed as previously described.[28,29] Briefly, mice were anesthetized with ketamine/xylazine and the left eye numbed with a drop of proparacaine. Following a lateral canthotomy, the optic nerve was exposed through an incision through the conjunctiva at the limbal junction. After a partial scraping of the scleral surface, the exposed optic nerve was clamped with N7 curved self-closing forceps (Fine Science Tools, Foster City, CA) for 3 seconds. After surgery, the eye was covered in antibiotic ointment and the mouse was allowed to recover. No procedure was done to the right eye of each mouse, because previous studies have shown that mock surgery does not affect ganglion cell morphology or number.[28]

For each experiment indicated here, a minimum of three mice were evaluated per time point, with the exception of the 18-month time point, in which two mice were examined.

Analysis of Cell and Nuclear Area

At appropriate times, mice were euthanized. Before enucleation, the superior region of the eye was marked on the cornea using an ophthalmic cautery (Fine Science Tools). Eyes were then removed and placed in PBS containing 4% paraformaldehyde at room temperature for 30 minutes, washed in PBS, and dissected to remove lens and cornea. Resulting eye cups were incubated overnight at 37°C in PBS containing 0.3% Triton X-100. After incubation, the retinas were removed, and a relaxing cut made along the superior axis from the periphery to the optic nerve head. Isolated retinas were incubated further in 3% H_2O_2 in 1% Na_2HPO_4 overnight at room temperature. Retinas were then wholemounted, ganglion cell layer exposed, onto Plus-charged microscope slides (Fisher Scientific, Pittsburgh, PA) using three more relaxing cuts. Both retinas from a single mouse were mounted onto the same slide. After partial drying, a coverslip was placed over the retinas and flattened with a 10-g weight. Retinas were allowed to dry for several hours to overnight. Dried retinas were then surface stained with Nissl stain (1% cresyl violet in 0.25% acetic acid). Staining time was generally no longer than 120 seconds, and checked visually under a light microscope. When the retinas were appropriately stained, they were differentiated in successive ethanol and xylene washes and coverslipped.

Images of stained cells were digitally captured using an Olympus BH-2 light microscope (Olympus, Center Valley, PA) equipped with a Pentax istD digital camera (Pentax, Montvale, NJ). All images were taken from the superior quadrant of the retinal wholemount under ×100 objective and oil emersion. A minimum of three fields for each retina were photographed, yielding a minimum of 300 cells analyzed from each retina. Only cells with round to oval nuclei and evidence of a nucleolus were considered as neurons and were measured (see Supplementary Material and Supplementary Fig. S1, http://www.iovs.org/lookup/suppl/doi:10.1167/iovs.11-9310/-/DCSupplemental). Vascular endothelial cell nuclei (spindle shaped) and cells with fragmented nuclei, indicating late-stage apoptosis, were not measured. Very small and condensed nuclei, which were presumed to be astrocytes and were present in both control and experimental retinas, were also not measured. At least three mice were imaged for each time point and condition reported here. Digital images were analyzed using Image Pro Plus v4.5 software (Media Cybernetics, Inc., Silver Spring, MD). Cell or nuclear area was determined by tracing around each object with the freehand cursor tool and area was calculated automatically by the program (measurements function), which had been calibrated from a stage micrometer photographed at the same magnification. An example of areas designated as either nuclear or cytoplasmic in a Nissl-stained cell is shown in the Supplementary Material and Supplementary Figure S1 (http://www.iovs.org/lookup/suppl/doi:10.1167/iovs.11-9310/-/DCSupplemental).

To better distinguish ganglion cells from other neurons in this layer, two methods were used. First, on Nissl-stained retinas, a subset of cells with obvious Nissl substance were compared with a subset of cells with no Nissl substance. Previously, Dräger and Olsen[30] reported that most Nissl-containing cells in the mouse retina were also identifiable as ganglion cells by retrograde labeling. Nissl staining has also been used as the principal criterion for identifying ganglion cells in primate studies focused on measuring atrophy of these cells in experimental glaucoma.[31] Second, ganglion cells were retrogradely labeled by placing a small piece of gel-foam soaked in ethanol containing 2% 1,1′-dioctadecyl-3,3,3′3′-tetramethylindocarbocyanine perchlorate (DiI; Anaspec, Inc., Freemont, CA) on the superior colliculus. After 3 days, animals underwent optic nerve crush surgery as described above. At selected time points, mice were euthanized and the retinas fixed and whole mounted. Retinas were counterstained with ddH_2O containing 300 ng/mL 4,6-diamidino-2-phenylindole (DAPI; Thermo Fisher Scientific, Rockford, IL) for 10 minutes and rinsed in PBS before being coverslipped. Cholinergic amacrine cells were separately identified in retinal wholemounts by the expression of the Tomato fluorescent protein. Digital images were captured at ×400 magnification using a Zeiss Axioplan 2 imaging microscope with Axiovision 4.6.3.0 software (Carl Zeiss MicroImaging, Inc., Thornwood, NY) and nuclear areas were determined as described above. Selections of nonganglion and ganglion cells were made principally from the peripheral superior retinas of mice, where cell density was lower and individual cell types were unambiguous. Approximately 40 cells of each type were identified in each retina examined and two to three mice were used for each time point investigated.

Evaluation of Nissl-staining or retrograde-labeling methods of selecting nonganglion and ganglion cell subsets yielded statistically similar estimates of nuclear atrophy for each cell population (*t*-test, $P = 0.667$ for nonganglion cells and $P = 0.333$ for ganglion cells).

Transmission Electron Microscopy

Wild-type and *Bax*-deficient mice were subjected to optic nerve crush, housed for 5 or 14 days, and then euthanized. Enucleated eyes were immersed briefly in 4% paraformaldehyde in PBS for 5 minutes, after which the anterior chambers and lenses were dissected away from each eye cup. A small region of the superior eye cup, including the retina, was then removed and placed in 2.5% glutaraldehyde, 2% paraformaldehyde in phosphate buffer (PB) overnight at 4°C. Tissue pieces were postfixed in 1% osmium tetroxide in PB, dehydrated in ethanol, and embedded in Epon epoxy. Sections (60–90 nm) were cut, stained with 50% ethanoic uranyl acetate and Reynold's lead citrate, and viewed using a Phillips CM120 transmission electron microscope (FEI Company, Hillsboro, OR).

Immunolabeling and Confocal Microscopy

Eye cups remaining after removal of a section of the superior region for electron microscopy were placed back into 4% paraformaldehyde in PBS for 45 minutes, followed by transfer into 0.4% paraformaldehyde in PBS overnight. Eye cups were then trimmed into hemispheres, equilibrated in 30% sucrose in PBS, and embedded in optimum temperature cutting compound (Tissue Tek, Torrance, CA). Frozen sections were cut at 5 μm and incubated with a rabbit polyclonal antiserum against acetylated histone H4 (Millipore, Inc., Billerica, MA) at a 1:100 dilution in PBS containing 4% BSA. Secondary antibody used was a goat anti-rabbit IgG conjugated to Texas Red (Jackson ImmunoResearch Laboratories, Inc., West Grove, PA) at a dilution of 1:1000 in the same buffer. After washing, sections were stained with DAPI before mounting. Sections were viewed using an inverted Nikon Eclipse Ti-E confocal microscope (Nikon Instruments, Melville, NY).

Quantitative Analysis of mRNA Abundance

Reverse-transcriptase quantitative PCR (qPCR) was conducted as described previously.[32] Briefly, wild-type and *Bax*$^{-/-}$ mice were subjected to optic nerve crush and housed for 14 days, at which time they were euthanized. Retinas were harvested and pooled from the left (crush) and right (control) eyes of five mice of each genotype, and processed to isolate total RNA using the acid phenol extraction method.[33] A total of 1.5 μg of this RNA was used to synthesize first-strand cDNA, which was used as a template for qPCR experiments. Primers and qPCR conditions have been reported elsewhere.[32] PCR was carried out on an ABI 7300 Real Time PCR System (Applied Biosystems, Foster City, CA). Data were obtained from triplicate samples for each target cDNA from each group of pooled retinas. Each individual qPCR reaction contained cDNA generated from approximately 1.9 pg of total polyA$^+$ RNA. Total transcript number was determined from an internal standard control of S16 cDNAs run on the same PCR plate. Loading differences were normalized to the number of S16 mRNA molecules present in each sample, which was also determined in the same run. The change in transcript expression between control and experimental retinas was calculated as the difference in transcript numbers between the experimental sample minus the control sample and represented as a percentage of the transcript amount in the control sample. Data were reported as the mean ± SD of these differences.

Statistical Analysis

Data sets of cell or nuclear area each satisfied requirements for a normal distribution, and statistical comparison between data sets were evaluated by one-way ANOVA. Comparisons of means were made using the Student's *t*-test. *P* values were considered significant at a level of 0.05, or less.

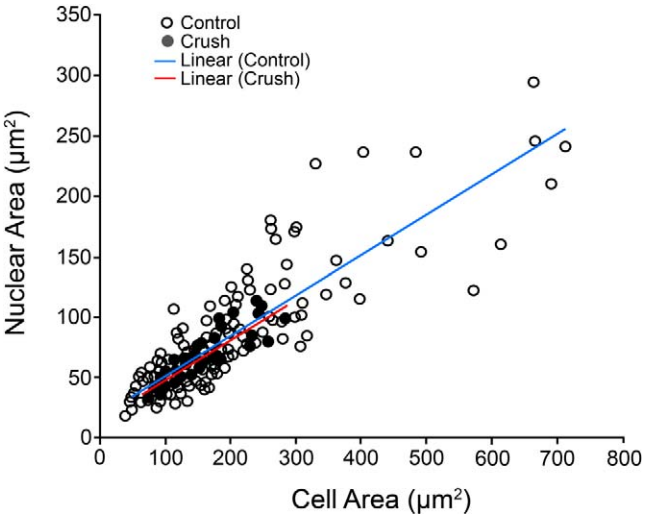

Figure 1. Scatter plot of cell soma area versus nuclear area. Cell soma areas and their corresponding nuclear areas were measured from Nissl-stained retinal wholemounts for cells that had clearly defined edges. Cell sizes were obtained from crush retinas at either 3 or 5 days after surgery to ensure that changes in cell size had ample time to occur after damage to the optic nerve. The best fit straight line for each data set is shown (*blue* for control and *red* for crush). Overall, control retinas contain more larger-sized cells than crush retinas (ANOVA, $P = 0.008$), but the linear relationships between the two variables are nearly identical for each data set ($y = 0.334x + 17.4$ and $y = 0.332x + 14.0$ for control and crush retinas, respectively, $P = 0.36$).

Results

Nuclear Size Is Proportional to Soma Size for Neurons in the Ganglion Cell Layer

Although both nuclear condensation and soma atrophy have been described independently for dying retinal ganglion cells, we examined if size changes of each metric were correlated. Nissl-stained mouse retinal wholemounts were prepared from normal eyes, or eyes subjected to optic nerve crush 3 and 5 days earlier. Measurements of cell area and nuclear area (see Supplementary Material and Supplementary Fig. S1 (http://www.iovs.org/lookup/suppl/doi:10.1167/iovs.11-9310/-/DCSupplemental) were made at random throughout the superior region of each retina and data were plotted as shown in Figure 1. Although crush retinas exhibited an overall decrease in the average cell size for this layer (ANOVA, $P = 0.008$), both groups showed a similar linear relationship between nuclear and soma size ($y = 0.334x + 17.4$ and $y = 0.332x + 14.0$ for control and crush retinas, respectively; $P = 0.36$, for comparison of slopes).

Time Course of Nuclear Atrophy in Wild-Type Mice after Optic Nerve Crush

To estimate the rate of nuclear atrophy, we euthanized wild-type mice at 1, 3, and 5 days after optic nerve crush, and measured nuclear areas of presumptive neurons (see Materials and Methods section) from Nissl-stained wholemounts. Representative images of retinas are shown in Figures 2A, 2C, 2E, 2G. In wild-type eyes, the first clear signs of apoptotic nuclei, evidenced by nuclear fragmentation, could be detected 5 days

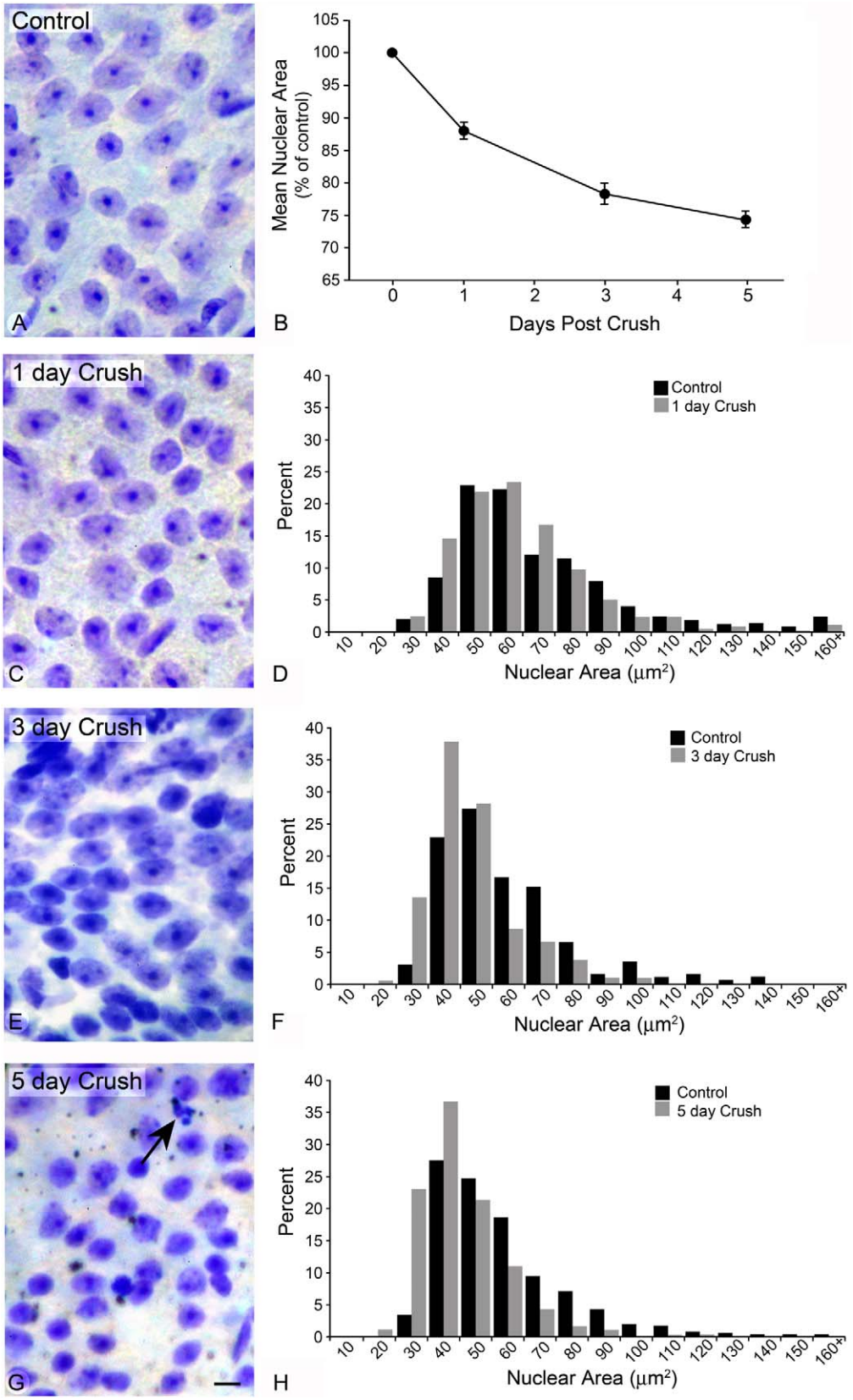

Figure 2. Time course of Nissl-stained retina wholemounts from wild-type mice after optic nerve crush. Representative images of Nissl-stained retinal wholemounts of mouse retinas before (**A**) and after optic nerve crush (**C**, **E**, **G**). All images were taken from the superior quadrants of each retina, approximately 1 mm from the optic nerve head and represent an area that has the same approximate density of cells. (**A**) Neuronal nuclei in control retinas appear plump and lightly stained with the exception of 1 or 2 prominent nucleoli. In preparations like these, vascular endothelial cells appear elongated, whereas astrocytes are often small and round. In both cases, the nuclei of these cells are densely stained. Shortly after crush,

the mean nuclear area of cells in the ganglion cell layer decreases relative to fellow control eyes (**B**). The decrease in size progresses to a maximum by 5 days after the surgery. At 1 day after crush (**C**), the nuclei are still relatively normal in appearance. A histograph of different cell sizes (**D**) shows a subtle loss of the largest cells and an increase in the proportion of small cells (control population, *black bars*; crush population, *grey bars*). (**E**) At 3 days after crush, nuclei are noticeably smaller and exhibit a greater proportion of darker staining, while histograph analysis shows a prominent increase in the proportion of smaller cells (**F**). (**G**) By 5 days after crush, the nuclei are noticeably smaller, and in wild-type mice, there are clearly signs of nuclear fragmentation (*arrow*). A histograph analysis (**H**) shows nearly complete loss of larger cells and a dramatic increase in the proportion of small cells. *Scale bar*: 10 μm. The decrease in nuclear area is significant at all 3 time points (ANOVA, $P < 0.0001$).

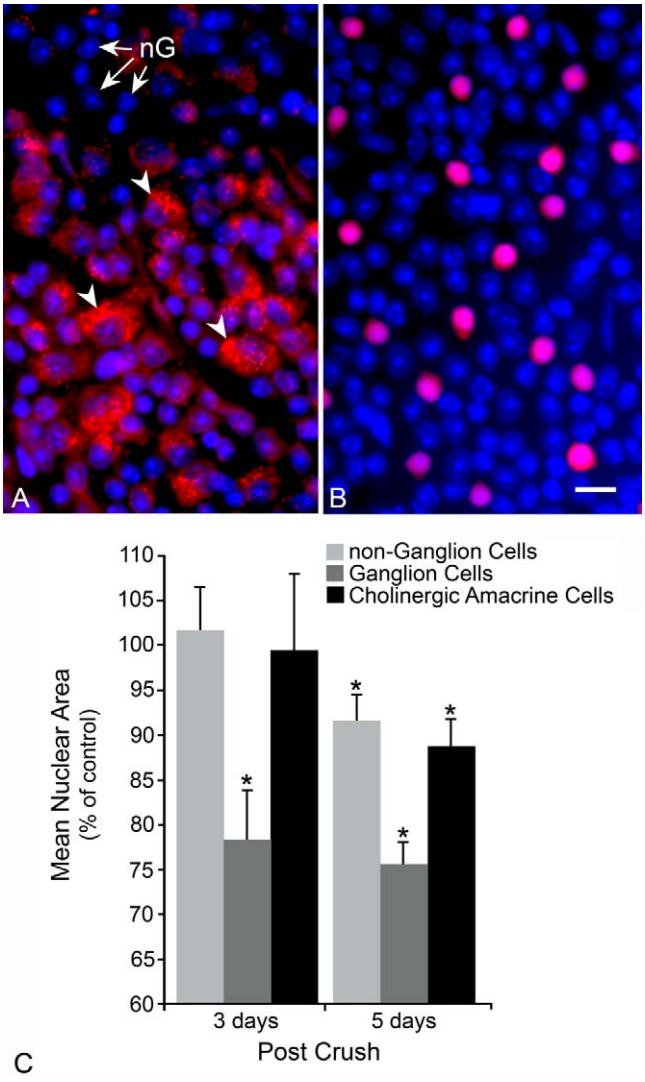

Figure 3. Atrophy of different neuronal populations in the ganglion cell layer. The nuclear sizes of distinct nonganglion and ganglion cell populations were measured in mouse retinas at 3 and 5 days after optic nerve crush. (**A**) Image of a section of a wholemount of the ganglion cell layer of a mouse retina, 5 days after crush. Ganglion cells were identified by retrograde labeling with DiI, while nuclei were identified by DAPI staining. DiI-negative cells with round nuclei and prominent nucleoli were selected as nonganglion cell neurons for analysis (nG, *arrows*). Cells that were unambiguously positive for retrograde DiI label (*red*) were selected for ganglion cells. Some ganglion cells also exhibited condensed DAPI staining (select examples highlighted with *arrowheads*). (**B**) Image of a section of a wholemounted retina of the ganglion cell layer of a *Rosa26R-LoxP-tdTomato* reporter mouse also transgenic for Cre recombinase under control of the choline acetyltransferase (*Tg(Chat-cre)GM24Gsat*). Cholinergic amacrine cells appear *red*. DAPI counterstain. *Scale bar* for (**A**, **B**): 10 μm. (**C**) Graph showing the mean change in nuclear area (±SEM, percentage of area of fellow control retinas) of nonganglion and ganglion cell subsets, and cholinergic amacrine cells, at 3 and 5 days after crush. At 3 days, only ganglion cells appear atrophied, while both nonganglion and ganglion cell populations are atrophied by 5 days. Populations of cells showing a significant change relative to control retina cell populations are indicated (*$P < 0.05$).

after crush (Fig. 2G). Fragmented nuclei were more numerous in retinas 7 days after crush (data not shown), consistent with earlier reports that peak TUNEL labeling[28] and the first significant loss of cells[33] are both detected at this time point. To quantify nuclear changes, a minimum of 900 cells was measured from control (OD) and experimental (OS) eyes at each time point. The mean (±SEM) nuclear area of experimental retinas, calculated as a percentage of the mean area of fellow control retinas, is shown in Figure 2B. Nuclear area, on average, decreases within 24 hours and continues to decline until day 5 (average of 25%), after which no further decrease was detected (data not shown). Frequency histographs of nuclear areas of presumptive neurons for both control and experimental eyes are shown for each time point (1 day, Fig. 2D; 3 days, Fig. 2F; 5 days, Fig. 2H). Over this time course, there is a clear shift to a greater proportion of smaller nuclei and decrease in the proportion of cells with large nuclei. Because cell loss is not prominent at these time points in the mouse crush model, this likely represents a decrease in the nuclear areas of existing cells.

Nuclear Atrophy Is Not Restricted to Ganglion Cells in the Ganglion Cell Layer

Retinal ganglion cells make up approximately 50% of the cells in the mouse ganglion cell layer (Schlamp CL, Nickells RW, unpublished observation, 2013). Others have reported that although mammalian retinal ganglion cells exhibit a greater amount of Nissl substance material,[30] Nissl staining does not readily distinguish between ganglion cells and displaced amacrine cells, which make up the remaining neuronal population. To verify what cell population in the ganglion cell layer is atrophying after optic nerve crush, we identified populations of nonganglion cells and ganglion cells by the presence of Nissl substance or with DiI introduced into the superior colliculus, 3 days before optic nerve surgery (see Materials and Methods section) (Fig. 3A). In control retinas, the nuclear area of nonganglion cells averaged 49.01 ± 11.92 μm^2, whereas ganglion cells averaged 73.82 ± 20.51 μm^2 (mean ± SD). At 3 days post optic nerve crush, nonganglion cells remained unchanged in nuclear area relative to control retinas ($P = 0.76$), while ganglion cell nuclei had decreased in area by 22.7% ($P = 0.01$). By 5 days, both nonganglion cells and ganglion cells exhibited significantly atrophied nuclei (8.4%, $P = 0.046$, for nonganglion cells and 24.4%, $P < 0.001$, for ganglion cells).

Back-labeling experiments suggest that amacrine cells (nonlabeled cells) also exhibit modest nuclear atrophy by 5 days after optic nerve crush. Alternatively, nonlabeled cells that atrophy may represent a subset of ganglion cells that were insufficiently labeled. To address this, we also evaluated the

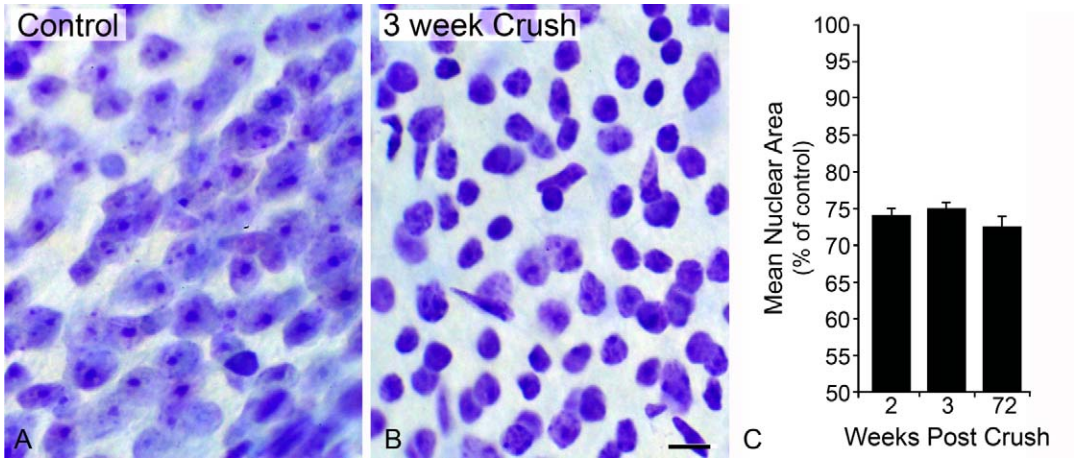

FIGURE 4. Nuclear area measurements in *Bax*$^{-/-}$ mice after optic nerve crush. To determine if nuclear shrinkage occurred before the committed step of the intrinsic apoptotic program, and before the activation of caspases, we examined nuclear area in *Bax*$^{-/-}$ mice after optic nerve crush. Retinal ganglion cells are absolutely dependent on BAX protein function to execute cell death after optic nerve crush.[34] Nissl-stained retinal wholemounts of control (**A**) and crush (**B**) retinas, 3 weeks after optic nerve damage. Neurons in the *Bax*$^{-/-}$ control retinas have a similar appearance to these cells in wild-type mice, including a plump appearance, lightly staining nucleoplasm, and densely staining nucleoli. After optic nerve crush, however, the nuclei are noticeably smaller and stain more intensely. Cell density between these images, however, remains similar because ganglion cells are arrested in the apoptotic program and have not been cleared. *Scale bar*: 10 μm. (**C**) Histographs of the mean change in nuclear area (±SEM relative to fellow control retinas) for *Bax*$^{-/-}$ mice at 2, 3, and 72 weeks after optic nerve crush. Each population is significantly smaller than control fellow eyes ($P < 0.001$ for each bar). *Bax*-deficient nuclei atrophy to a similar extent as nuclei in wild-type mice (approximately 25% atrophy, compare to Fig. 2B), and appear to remain atrophied indefinitely.

atrophy of cholinergic amacrine cells in this layer, labeled by the activation of the *Rosa26R-LoxP-tdTomato* reporter gene by the specific expression of Cre recombinase in these cells (Fig. 3B). Fluorescently labeled cholinergic amacrine cells exhibited no significant nuclear atrophy at 3 days after optic nerve crush ($P = 0.34$), but were significantly smaller by 5 days (11.2% decrease, $P < 0.001$) (Fig. 3C).

Nuclear Atrophy Occurs in *Bax*-Deficient Mice

The data collected from wild-type mice indicate that nuclear atrophy is a result of a rapid signaling mechanism between damaged axons in the optic nerve and the cell soma, and therefore may precede the point of BAX activation in the apoptotic program. *Bax*$^{-/-}$ mice provide a valuable tool to examine early apoptotic changes in ganglion cells, because these cells are completely blocked from executing the apoptotic program in response to optic nerve crush,[9,34] surviving for as long as 18 months after optic nerve damage.[35] To evaluate atrophy in *Bax*$^{-/-}$ cells, we repeated optic nerve crush experiments on knockout mice and quantified nuclear shrinkage. Five days after optic nerve crush, *Bax*$^{+/+}$ and *Bax*$^{-/-}$ cells both shrank a mean of 27.0% and 25.9%, respectively (data not shown). Nuclei in *Bax*$^{-/-}$ mice appear to remain atrophied indefinitely, exhibiting a mean area that is centered approximately 26% smaller than control retinas at 2 to 3 weeks, and even 18 months after optic nerve crush (Fig. 4, $P < 0.001$ versus control retinas for all time points). Nearly identical results for nuclear atrophy were observed at 2 and 3 weeks in *Bax*$^{+/-}$ mice (data not shown), which exhibit a retarded rate of ganglion cell loss after optic nerve crush.[35]

Ganglion cells were also distinguished from nonganglion cells in *Bax*$^{+/-}$ mice by DiI back-labeling. Similar results to those obtained in wild-type animals at 5 days after optic nerve crush were observed in these mice, with nonganglion cells exhibiting a 11.0% decrease in nuclear area ($P = 0.008$) and ganglion cells exhibiting a 26.2% decrease ($P < 0.001$).

Heterochromatin Formation, Histone Deacetylation, and Silencing of Ganglion Cell Gene Expression Occur in Both Wild-Type and *Bax*-Deficient Mice

Nuclear shrinkage is one aspect of nuclear atrophy, but other changes may include alterations in chromatin structure and gene expression. Transmission electron microscopic studies have documented that the conversion of euchromatin to heterochromatin is a consistent feature of affected ganglion cells in both nonhuman primate and mouse models of glaucoma.[9,36] To better evaluate the formation of heterochromatin, particularly in *Bax*-deficient cells, we performed optic nerve crush and surveyed nuclei in the ganglion cell layer by transmission electron microscopy at 5 and 14 days after surgery. In both *Bax*$^{+/+}$ and *Bax*$^{-/-}$ mice, the ganglion cell layers of control retinas were principally populated by neurons containing large round or oval nuclei, with minimal heterochromatin staining and a prominent nucleolus (Figs. 5A, 5B, wild-type and knockout mouse, respectively). In wild-type mice, 5 days after optic nerve crush, most neuronal nuclei appeared convoluted and exhibited moderate levels of heterochromatin (Fig. 5C). A small percentage of cells (approximately 1%–2%) were in the late stages of apoptotic degeneration, with completely heterochromatic and fragmented nuclei. These nuclear fragments also lacked a nuclear envelope (Fig. 5E). Similarly, nuclei in the ganglion cell layers of *Bax*$^{-/-}$ mice were more likely to appear convoluted and contain heterochromatin at both 5 and 14 days after optic nerve crush (Figs. 5D, 5F). Cells with convoluted nuclei in the *Bax*$^{-/-}$ mice always contained intact nuclear envelopes, complete with nuclear pore structures (Fig. 6). A second feature typical of cells with altered nuclei in both wild-type and *Bax*$^{-/-}$ mice was the presence of numerous electron-dense inclusions that resembled autophagosomes, or their precursors, phagophors (Fig. 6).[37]

In separate experiments, we also examined the loss of histone acetylation in nuclei of the ganglion cell layer in *Bax*-

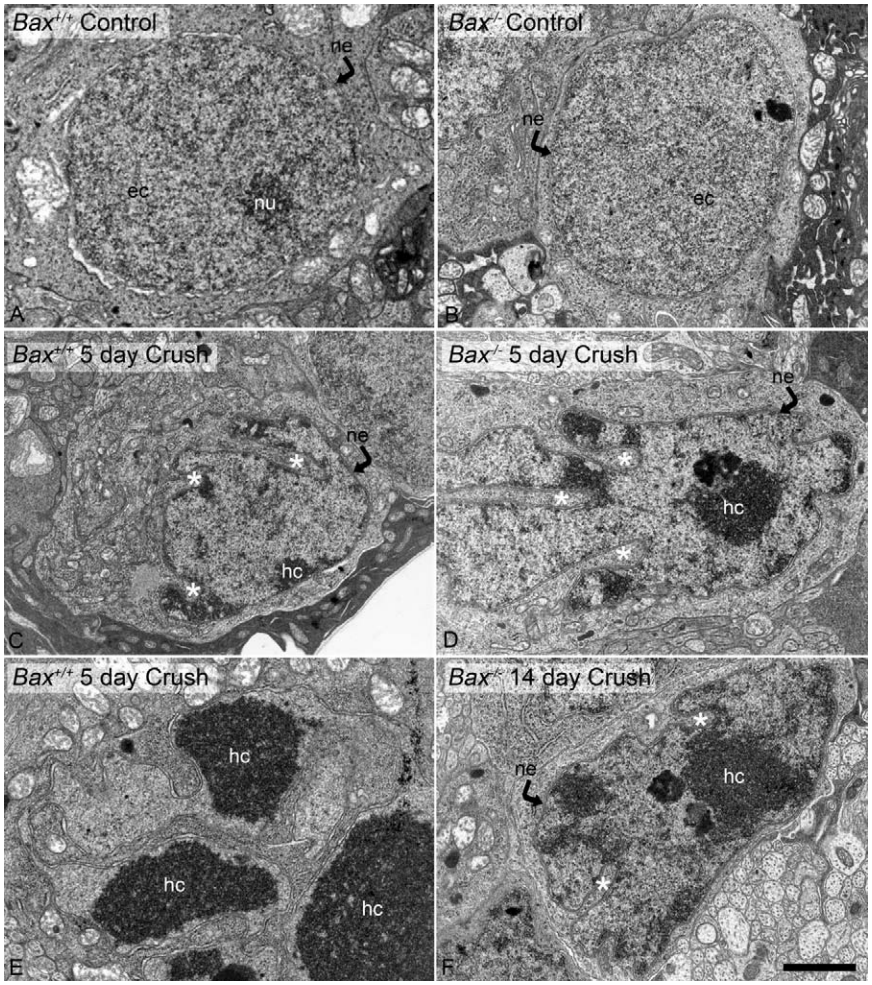

Figure 5. Ultrastructure of ganglion cell layer nuclei in wild-type and *Bax*$^{-/-}$ mice after optic nerve crush. Transmission electron micrographs of cells in the ganglion cell layer of wild-type (**A**, **C**, **E**) and *Bax*$^{-/-}$ (**B**, **D**, **F**) mice. The most prominent nuclear appearance in the ganglion cell layer of control retinas (**A**, **B**) was of round or slightly oval nuclei with a small electron-dense nucleolus (nu) and uniformly staining nucleoplasm, typical of euchromatin (ec). After optic nerve crush, these nuclei became less obvious and were replaced by nuclei exhibiting highly convoluted sinuses (*asterisks* in [**C**, **D**, **F**]). Although these nuclei still contained an intact nuclear envelope (ne), they also exhibited increased deposition of electron-dense heterochromatin (hc). Some nuclei in wild-type mice also appeared completely electron dense and fragmented (**E**), with no evidence of an intact nuclear envelope. Nuclei in *Bax*$^{-/-}$ mice never reached this stage of nuclear condensation, and appeared similar at 5 and 14 days after crush. *Scale bar*: 1.5 μm.

deficient mice. Immunofluorescent staining of acetylated histone H4 at 5 and 14 days post crush revealed a substantial decrease in H4 acetylation in nuclei of cells in the ganglion cell layers of both wild-type and *Bax*$^{-/-}$ mice (Fig. 7). Nuclei with reduced or absent acetylation also appeared condensed and abnormal when examined with a DAPI counterstain.

Last, concomitant with histone deacetylation and nuclear atrophy, wild-type retinal ganglion cells have been reported to exhibit a rapid silencing of normal cell gene expression before cell soma loss.[32,33,38–42] We had previously also observed a similar decrease in mRNA levels for the putative ganglion cell marker gene *Thy1* in *Bax*-deficient mice.[33] Because *Thy1* may also be a marker for Müller cells in damaged retinas,[43] we expanded our quantitative analysis to include other established ganglion cell markers (*Nrn1* and *Sncg*) as well as genes reportedly upregulated in damaged ganglion cells (*Hsp27*, *Bim*, and *Gap43*). Quantitative PCR analysis was conducted on retinas at 14 days after optic nerve crush because ganglion cell loss in wild-type mice is only partially completed at this time (Fig. 8). Both wild-type and *Bax*-deficient mice showed statistically identical decreases in three genes normally expressed in healthy ganglion cells ($P > 0.05$, *Bax*$^{+/+}$ versus *Bax*$^{-/-}$ retinas). Wild-type mice, however, exhibited increased expression of the three stress-response genes that were minimally upregulated or downregulated in *Bax*$^{-/-}$ mice ($P < 0.001$, *Bax*$^{+/+}$ versus *Bax*$^{-/-}$ retinas).

Discussion

Here, we demonstrate that cell atrophy, particularly nuclear shrinkage, occurs rapidly after an acute damaging stimulus to the optic nerve in mice. Because both the somas and nuclei of cells appear to decrease in size uniformly, nuclear area may be a useful surrogate to measure the AVD in this tissue. Using *Bax*-deficient mice to arrest the process of ganglion cell apoptosis, we also show that nuclear shrinkage occurs before the committed step of the apoptotic pathway, demonstrating that, at least initially, this process is independent of caspase activation. This may represent the first phase of the AVD described by Bortner and colleagues,[17,22] which precedes a later caspase-dependent phase in some cells. These data are

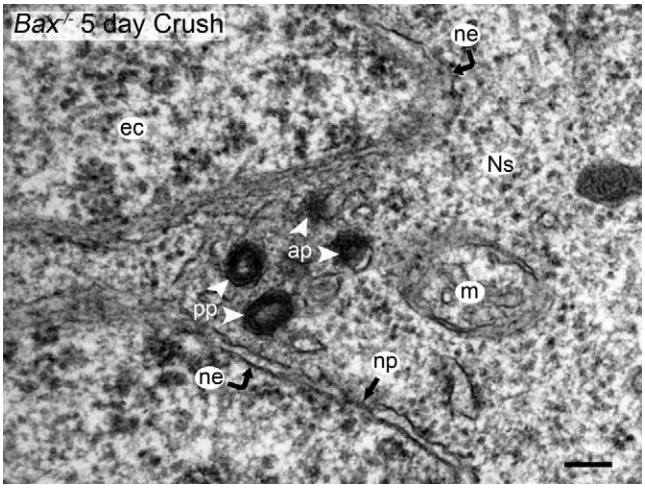

FIGURE 6. High magnification of a *Bax*$^{-/-}$ cell after optic nerve crush. Detail of the nuclear envelope and cytoplasm of a *Bax*$^{-/-}$ cell 5 days after optic nerve crush. In both wild-type and *Bax*$^{-/-}$ retinas, cells affected by optic nerve crush accumulated electron-dense vesicles, which appeared to be autophagosomes (ap) or their precursors, phagophores (pp). Otherwise, the cytoplasm appeared normal with granular-appearing polyribosomes (Nissl-substance, Ns) and mitochondria (m). These cells also exhibited relatively normal-appearing rough endoplasmic reticulum and Golgi (not shown). Convoluted nuclei contained both light-staining euchromatin (ec) and electron-dense heterochromatin. These nuclei had intact nuclear envelopes (ne), with normal-appearing nuclear pore structures (np). Affected *Bax*$^{-/-}$ cells appeared similar in retinas both 5 and 14 days after optic nerve crush. *Scale bar*: 130 nm.

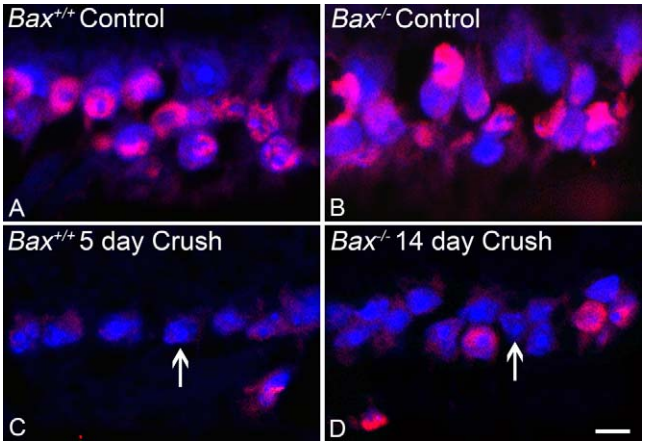

FIGURE 7. Immunofluorescent staining for acetyl histone H4 in nuclei of wild-type and *Bax*$^{-/-}$ mice after optic nerve crush. Confocal optical sections through the ganglion cell layer of control and experimental mouse retinas after optic nerve crush. Sections were immunostained for acetylated histone H4 (*red*) and counterstained with DAPI (*blue*). Only merged images are shown. (**A**, **C**) Sections from wild-type mice 5 days after crush. (**B**, **D**) Sections from *Bax*$^{-/-}$ mice 14 days after crush. In control retinas, most nuclei stain strongly for acetylated H4 and have normal-appearing nuclei by DAPI staining. After crush, however, nuclei exhibiting increases in DNA condensation (more intense and mottled DAPI staining; representative nuclei highlighted by *arrows* in [**C**, **D**]) are weakly positive for acetylated H4. This pattern of histone deacetylation was also evident in *Bax*$^{-/-}$ samples collected 5 days after crush (data not shown). *Scale bar*: 10 μm.

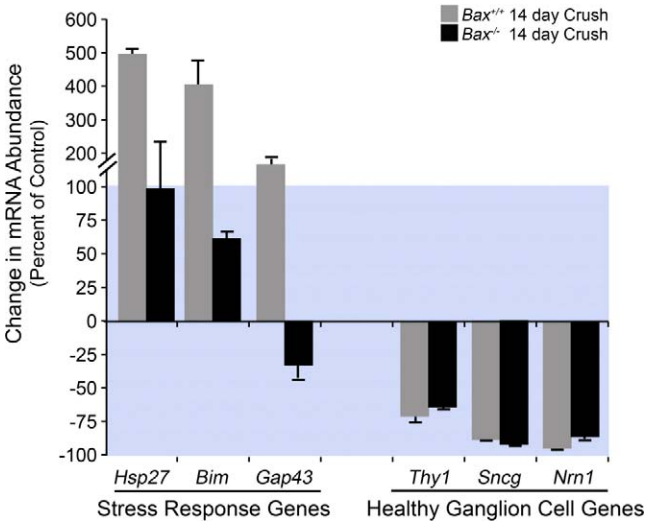

FIGURE 8. Histographs of retinal ganglion cell transcript abundance after optic nerve crush. The levels of six different mRNAs were analyzed in the retinas of wild-type and *Bax*$^{-/-}$ mice, 2 weeks after optic nerve crush. Three of the transcripts (*Hsp27*, *Bim*, and *Gap43*) are indicative of ganglion cell stress responses. The other three transcripts (*Thy1*, *Sncg*, and *Nrn1*) are indicative of normal healthy adult ganglion cells. The data are represented as the change in transcript abundance between experimental and control samples, and expressed as a percentage of transcript numbers in control samples (mean ± SD of triplicate samples for each target cDNA). After optic nerve crush, wild-type mice exhibit an increase in stress-related gene expression, and a decrease in the mRNAs normally expressed in ganglion cells. Although *Bax*$^{-/-}$ ganglion cells also exhibit a downregulation of normal gene expression statistically identical to wild-type mice ($P > 0.05$, for each transcript), stress-related gene expression is dramatically muted ($P < 0.001$ for each bar). Because there is a dramatic difference in the upregulation of stress response genes relative to downregulated genes, the data are shown using an expanded scale between 0% and ±100% change (*blue-shaded region*).

consistent with a previous observation that motoneurons also atrophy in *Bax*-deficient mice after axotomy of the sciatic nerve.[44]

From the perspective of cell susceptibility in glaucomatous damage, there is anatomical evidence that many subtypes of ganglion cells atrophy and shrink before dying in response to optic nerve damage, including glaucoma.[23–25,45–48] This contrasts with earlier studies, which indicated that magnocellular ganglion cells were more susceptible to glaucomatous atrophy.[31,49,50] It should be noted that we did not selectively measure nuclear changes in different ganglion cell subtypes, and our data cannot reveal that nuclei shrank at a uniform rate throughout the ganglion cell layer. As a consequence, we cannot conclude that larger cells were more or equally affected. Nevertheless, the assumption that larger magnocellular cells are more sensitive should be revisited, as this assumption was predicated on data collected by measuring cell sizes in retinal wholemounts in a way similar to what we have done in this report. Thus, a uniform decrease in the size of all ganglion cells could be misinterpreted as a selective loss of larger cells.

Our data also indicate that both ganglion cells and presumptive other neurons in the ganglion cell layer atrophy, albeit at different rates. Ganglion cells appear to be the most profoundly affected, and our observations suggest that their nuclei atrophy earlier than nonganglion cells after optic nerve crush. The most abundant cell types in the nonganglion cell population are displaced amacrine cells.[51,52] Using mice with genetically labeled cholinergic amacrine cells, which make up

approximately 19.5% of the displaced amacrine cell population,[51] we confirm that at least one subset of these cells exhibits a degree of nuclear atrophy. Although there is no evidence that amacrine cells die after damage to the optic nerve, they have been reported to exhibit depletion of neurotransmitters after axotomy.[53] This may be a result of the loss of synapse formation with ganglion cell somas and dendrites, which retract shortly after optic nerve damage.[24,27] Because amacrine cells make up the large majority of presynaptic contacts with ganglion cells in rod-rich retinas, such as in the mouse,[52] it is conceivable that loss of these contacts stimulates a modest atrophy response in these neurons as well. In this model, we would predict that atrophy of ganglion cells would necessarily precede atrophy in amacrines, which is consistent with the timing of our observations.

Changes in Chromatin Structure and Gene Function in Damaged Ganglion Cells

Nuclear atrophy, defined as nuclear shrinkage, was also investigated at the ultrastructural level. Affected cells accumulate heterochromatin and exhibit a dramatic morphological change in nuclear structure. Rather than shrinking uniformly, the nucleus appears to collapse, resulting in the formation of numerous involutions. An analogy would be a deflated basketball, which would result in infolding of the ball rather than a uniform decrease in size. Overall, these involutions result in a nuclear structure similar to that described for amacrine cells,[54] which also have highly involuted nuclei, but lack the heterochromatic regions. A similar ultrastructural appearance was described previously for dying retinal ganglion cells in the chick retina after tectal lesion[55] and rat ganglion cells after optic nerve crush.[56]

The condensation of euchromatin into heterochromatin may be one mechanism that precipitates the collapse of the nuclei of damaged cells. One aspect of chromatin changes, global histone H4 deacetylation, does occur in both wild-type and *Bax*-deficient mice, and this process has been linked to the formation of heterochromatin.[57–59] It is not clear, however, if deacetylation is a causative mechanism or a consequence of other events leading to heterochromatin formation and atrophy. Efforts to block chromatin condensation and nuclear shrinkage by preventing the activity of histone deacetylases were unsuccessful (data not shown), suggesting the latter interpretation. Heterochromatin formation during apoptosis may be a distinct process from similar chromatin changes observed during mitosis.[14,60] Studies of pericentromeres in mice indicate that heterochromatin formation first requires extensive methylation of lysine 9 on histone H3 (H3K9me2). This provides a binding site for Heterochromatin Protein 1 (HP1) to bind and recruit histone deacetylases for hypoacetylation. The association between HP1 localization and nuclear apoptotic is not well studied, however, and mice with suppressed expression of *Hp1α* (*Cbx5*) show no overt phenotypic abnormalities associated with dysregulation of apoptosis, although embryo viability is reduced in homozygous mutant animals.[61]

Hendzel and colleagues[58] suggested that condensation of heterochromatin in dying cells was facilitated by the rapid digestion of hypersensitive euchromatin, which then leaked into the cytoplasm. This was predicted to precede internucleosomal DNA degradation of nucleases that require caspase activation and is a hallmark of apoptosis. Other groups, however, have reported that nuclease activity is not required for condensation.[62]

Another critical feature of nuclear changes in apoptotic cells is the breakdown of the nuclear lamina, which is facilitated by the proteolytic cleavage of nuclear lamins.[14] Replacing wild-type lamins with proteins that are resistant to cleavage retard the condensation process.[14] Several reports have linked lamin cleavage to caspase 6 activation.[60] Although it is conceivable that lamin breakdown is a mechanism that facilitates nuclear shrinkage, the observation that nuclei also exhibit condensation and atrophy in *Bax*-deficient cells is not consistent with this hypothesis. Protease activation, from caspases or calpains, is absent or suppressed in cells reliant on the intrinsic apoptotic pathway (such as retinal ganglion cells in this experimental paradigm) if BAX activation does not occur.[63–65] We have preliminary data showing that lamin staining remains robust in *Bax*-deficient cells after crush (data not shown). Similarly, lamins play a critical role in maintaining the integrity of the nuclear envelope and their breakdown is required for dissolution of this structure during apoptosis.[66,67] We observe that not only do atrophied nuclei in the ganglion cell layer of *Bax*-deficient mice retain a normal nuclear envelope, but these cells are still present in the retina many months after crush. These observations argue that the earliest nuclear changes in apoptotic cells may occur by a mechanism not reliant on protease and/or nuclease activities, although this is a hypothesis that remains to be tested. *Bax*-knockout mice could be a useful resource to study the early events associated with nuclear/chromatin changes.

We examined the transcript levels of two different gene sets to evaluate transcriptional changes in atrophied nuclei of $Bax^{-/-}$ ganglion cells. The first set of genes was designed to examine gene expression of normal healthy ganglion cells and included three "ganglion cell–specific" genes (*Thy1*, *Sncg*, and *Nrn1*).[40,41,68] A variety of reports indicate that all of these genes are downregulated in damaged ganglion cells.[33,39–41,69,70] In addition to these genes, we also examined a second set of genes (*Hsp27*, *Bim*, and *Gap43*) that are upregulated in damaged ganglion cells.[71–74] The quantitative analysis of these mRNAs in $Bax^{-/-}$ mice revealed that these cells undergo silencing of normal gene expression, similar to that observed in wild-type cells. Alternatively, stress response ganglion cell gene expression is muted in $Bax^{-/-}$ retinas. This suggests that blocking the full execution of apoptosis is able to attenuate gene expression needed to complete the program. A caveat of this analysis is that it does not evaluate housekeeping gene expression in surviving ganglion cells. Because $Bax^{-/-}$ ganglion cells appear to survive indefinitely,[35] it is reasonable to assume that they retain some level of basal expression of these housekeeping genes. Our interpretation of the results reported here is that silencing of ganglion cell–specific gene expression is a fundamental early response to damage, as the products of these genes are no longer vital to executing the apoptotic program.

In conclusion, the observations of nuclear changes in *Bax*-deficient cells reflects previous observations that chromatin condensation may be a two-stage process, the first being independent of caspase and nuclease activation, but a fundamental process required to suppress ganglion cell gene expression in preparation for further execution of the apoptotic program. Further nuclear changes then are likely a consequence of caspase-dependent activation of endonucleases[75] and nuclear lamina proteolysis.[14,60]

Acknowledgments

The authors thank Ben August and Lance Rodenkirch for assistance with studies involving transmission electron microscopy and confocal imaging, respectively, and Brian Yandell for advice on statistical analyses.

References

1. Nickells RW. Retinal ganglion cell death in glaucoma: the how, the why, and the maybe. *J Glaucoma*. 1996;5:345–356.
2. Nickells RW. From ocular hypertension to ganglion cell death: a theoretical sequence of events leading to glaucoma. *Can J Ophthalmol*. 2007;42:278–287.
3. Morrison JC, Cepurna WO, Jia L, Aubert J, Johnson EC. Mechanism of focal optic nerve injury from elevated intraocular pressure. *Invest Ophthalmol Vis Sci*. 2002;43: U813.
4. Morrison JC, Johnson EC, Cepurna WA, Jia L. Understanding mechanisms of pressure-induced optic nerve damage. *Prog Retin Eye Res*. 2005;24:217–240.
5. Johnson EC, Jia L, Cepurna WA, Doser TA, Morrison JC. Global changes in optic nerve head gene expression after exposure to elevated intraocular pressure in a rat glaucoma model. *Invest Ophthalmol Vis Sci*. 2007;48:3161–3177.
6. Nguyen JV, Soto I, Kim K-Y, et al. Myelination transition zone astrocytes are constitutively phagocytic and have synuclein dependent reactivity in glaucoma. *Proc Natl Acad Sci U S A*. 2011;108:1176–1181.
7. Whitmore AV, Libby RT, John SWM. Glaucoma: thinking in new ways—a role for autonomous axonal self-destruction and compartmentalised processes? *Prog Retin Eye Res*. 2005;24: 639–662.
8. Howell GR, Macalinao DG, Sousa GL, et al. Molecular clustering identifies complement and endothelin induction as early events in a mouse model of glaucoma. *J Clin Invest*. 2011;121:1429–1444.
9. Libby RT, Li Y, Savinova OV, et al. Susceptibility to neurodegeneration in glaucoma is modified by Bax gene dosage. *PLoS Genet*. 2005;1:17–26.
10. Whitmore AV, Lindsten T, Raff MC, Thompson CB. The proapoptotic proteins Bax and Bak are not involved in Wallerian degeneration. *Cell Death Differ*. 2003;10:260–261.
11. Howell GR, Libby RT, Jakobs TC, et al. Axons of retinal ganglion cells are insulted in the optic nerve early in DBA/2J glaucoma. *J Cell Biol*. 2007;179:1523–1537.
12. Barros LF, Hermosilla T, Castro J. Necrotic volume increase and the early physiology of necrosis. *Comp Biochem Physiol*. 2001;130:401–409.
13. Kerr JFR, Wyllie AH, Currie AR. Apoptosis: a basic biological phenomenon with wide-ranging implications in tissue kinetics. *Br J Cancer*. 1972;26:239–257.
14. Rao L, Perez D, White E. Lamin proteolysis facilitates nuclear events during apoptosis. *J Cell Biol*. 1996;135:1441–1455.
15. Wolf CM, Reynolds JE, Morana SJ, Eastman A. The temporal relationship between protein phosphatase, ICE/CED-3 proteases, intracellular acidification, and DNA fragmentation in apoptosis. *Exp Cell Res*. 1997;230:22–27.
16. Bortner CD, Cidlowski JA. Cell shrinkage and monovalent cation fluxes: role in apoptosis. *Arch Biochem Biophys*. 2007; 462:176–188.
17. Bortner CD, Sifre MI, Cidlowski JA. Cationic gradient reversal and cytoskeleton-independent volume regulatory pathways define an early stage of apoptosis. *J Biol Chem*. 2008;283: 7219–7229.
18. Szabo I, Zoratti M, Gulbins E. Contribution of voltage-gated potassium channels to the regulation of apoptosis. *FEBS Lett*. 2010;584:2049–2056.
19. Hernandez-Enriquez B, Arellano RO, Moran J. Role for ionic fluxes on cell death and apoptotic volume decrease in cultured cerebellar granule neurons. *Neuroscience*. 2010; 167:298–311.
20. Pal SK, Hartnett KA, Nerbonne JM, Levitan ES, Aizenman E. Mediation of neuronal apoptosis by Kv2.1-encoded potassium channels. *J Neurosci*. 2003;23:4798–4802.
21. Redman PT, He K, Hartnett KA, et al. Apoptotic surge of potassium currents is mediated by p38 phosphorylation of Kv2.1. *Proc Natl Acad Sci U S A*. 2007;104:3568–3573.
22. Bortner CD, Cidlowski JA. Caspase independent/dependent regulation of K^+, cell shrinkage, and mitochondrial membrane potential during lymphocyte apoptosis. *J Biol Chem*. 1999; 274:21953–21962.
23. Weber AJ, Kaufman PL, Hubbard WC. Morphology of single ganglion cells in the glaucomatous primate retina. *Invest Ophthalmol Vis Sci*. 1998;39:2304–2320.
24. Weber AJ, Harman CD, Viswanathan S. Effects of optic nerve injury, glaucoma, and neuroprotection on the survival, structure, and function of ganglion cells in the mammalian retina. *J Physiol*. 2008;586:4393–4400.
25. Jakobs TC, Libby RT, Ben Y, John SWM, Masland RH. Retinal ganglion cell degeneration is topological but not cell type specific in DBA/2J mice. *J Cell Biol*. 2005;171:313–325.
26. Weber AJ, Harman CD. BDNF preserves the dendritic morphology of a and b ganglion cells in the cat retina after optic nerve injury. *Invest Ophthalmol Vis Sci*. 2008;49:2456–2463.
27. Leung CK, Weinreb RN, Li ZW, et al. Long-term imaging and measurement of dendritic shrinkage of retinal ganglion cells. *Invest Ophthalmol Vis Sci*. 2011;52:1539–1547.
28. Li Y, Schlamp CL, Nickells RW. Experimental induction of retinal ganglion cell death in adult mice. *Invest Ophthalmol Vis Sci*. 1999;40:1004–1008.
29. Li Y, Semaan SJ, Schlamp CL, Nickells RW. Dominant inheritance of retinal ganglion cell resistance to optic nerve crush in mice. *BMC Neurosci*. 2007;8:19.
30. Dräger UC, Olsen JF. Ganglion cell distribution in the retina of the mouse. *Invest Ophthalmol Vis Sci*. 1981;20:285–293.
31. Glovinsky Y, Quigley HA, Dunkelberger GR. Retinal ganglion cell loss is size dependent in experimental glaucoma. *Invest Ophthalmol Vis Sci*. 1991;32:484–491.
32. Pelzel HR, Schlamp CL, Nickells RW. Histone H4 deacetylation plays a critical role in early gene silencing during neuronal apoptosis. *BMC Neurosci*. 2010;11:62.
33. Schlamp CL, Johnson EC, Li Y, Morrison JC, Nickells RW. Changes in Thy1 gene expression associated with damaged retinal ganglion cells. *Mol Vis*. 2001;7:192–201.
34. Li Y, Schlamp CL, Poulsen KP, Nickells RW. Bax-dependent and independent pathways of retinal ganglion cell death induced by different damaging stimuli. *Exp Eye Res*. 2000;71:209–213.
35. Semaan SJ, Li Y, Nickells RW. A single nucleotide polymorphism in the Bax gene promoter affects transcription and influences retinal ganglion cell death. *ASN Neuro*. 2010;2: e00032.
36. Quigley HA, Nickells RW, Kerrigan LA, et al. Retinal ganglion cell death in experimental glaucoma and after axotomy occurs by apoptosis. *Invest Ophthalmol Vis Sci*. 1995;36:774–786.
37. Kang R, Zeh HJ, Lotze MT, Tang D. The Beclin 1 network regulates autophagy and apoptosis. *Cell Death Differ*. 2011;18: 571–580.
38. Weishaupt JH, Klocker N, Bahr M. Axotomy-induced early down-regulation of POU-IV class transcription factors Brn-3a and Brn-3b in retinal ganglion cells. *J Mol Neurosci*. 2005;26: 17–25.
39. Huang W, Fileta J, Guo Y, Grosskreutz CL. Downregulation of Thy1 in retinal ganglion cells in experimental glaucoma. *Curr Eye Res*. 2006;31:265–271.
40. Yang Z, Quigley HA, Pease ME, et al. Changes in gene expression in experimental glaucoma and optic nerve transection: the equilibrium between protective and detrimental mechanisms. *Invest Ophthalmol Vis Sci*. 2007;48: 5539–5548.
41. Soto I, Oglesby E, Buckingham BP, et al. Retinal ganglion cells downregulate gene expression and lose their axons within the

optic nerve head in a mouse glaucoma model. *J Neurosci*. 2008;28:548–561.

42. Pelzel HR, Schlamp CL, Waclawski M, Shaw MK, Nickells RW. Silencing of Fem1c^{R3} gene expression in the DBA/2J mouse precedes retinal ganglion cell death and is associated with histone deacetylase activity. *Invest Ophthalmol Vis Sci*. 2012; 53:1428–1435.
43. Dabin I, Barnstable CJ. Rat retinal Müller cells express Thy-1 following neuronal cell death. *Glia*. 1995;14:23–32.
44. Sun W, Oppenheim RW. Response of motoneurons to neonatal sciatic nerve axotomy in Bax-knockout mice. *Mol Cell Neurosci*. 2003;24:875–886.
45. Misantone LJ, Gershenbaum M, Murray M. Viability of retinal ganglion cells after optic nerve crush in rats. *J Neurocytol*. 1984;13:449–465.
46. Morgan JE, Uchida H, Caprioli J. Retinal ganglion cell death in experimental glaucoma. *Br J Ophthalmol*. 2000;84:303–310.
47. Morgan JE. Retinal ganglion cell shrinkage in glaucoma. *J Glaucoma*. 2002;11:365–370.
48. Buckingham BP, Inman DM, Lambert W, et al. Progressive ganglion cell degeneration precedes neuronal loss in a mouse model of glaucoma. *J Neurosci*. 2008;28:2735–2744.
49. Glovinsky Y, Quigley HA, Pease ME. Foveal ganglion cell loss is size dependent in experimental glaucoma. *Invest Ophthalmol Vis Sci*. 1993;34:395–400.
50. Quigley HA, Dunkelberger GR, Green WR. Retinal ganglion cell atrophy correlated with automated perimetry in human eyes with glaucoma. *Am J Ophthalmol*. 1989;107:453–464.
51. Jeon C-J, Strettoi E, Masland RH. The major cell populations of the mouse retina. *J Neurosci*. 1998;18:8936–8946.
52. Rodieck RW. *The First Steps in Seeing*. Sunderland, MA: Sinauer Associates, Inc.; 1998.
53. Kielczewski JL, Pease ME, Quigley HA. The effect of experimental glaucoma and optic nerve transection on amacrine cells in the rat retina. *Invest Ophthalmol Vis Sci*. 2005;46:3188–3196.
54. Hogan MJ, Alvarado JA, Weddell JE. *Histology of the Human Eye*. Philadelphia, PA: W. B. Saunders Company; 1971.
55. Borsello T, Mottier V, Castagne V, Clarke PGH. Ultrastructure of retinal ganglion cell death after axotomy in chick embryos. *J Comp Neurol*. 2002;453:361–371.
56. Barron KD, Dentinger MP, Krohel G, Easton SK, Mankes R. Qualitative and quantitative ultrastructural observations on retinal ganglion cell layer of rat after intraorbital optic nerve crush. *J Neurocytol*. 1986;15:345–362.
57. O'Neill LP, Turner BM. Histone H4 acetylation distinguishes coding regions of the human genome from heterochromatin in a differentiation-dependent but transcription-independent manner. *EMBO J*. 1995;14:3946–3957.
58. Hendzel MJ, Nishioka WK, Raymond Y, et al. Chromatin condensation is not associated with apoptosis. *J Biol Chem*. 1998;273:24470–24478.
59. Shahbazian MD, Grunstein M. Functions of site-specific histone acetylation and deacetylation. *Ann Rev Biochem*. 2007;76:75–100.
60. Ruchaud S, Korfali N, Villa P, et al. Caspase-6 gene disruption reveals a requirement for lamin A cleavage in apoptotic chromatin condensation. *EMBO J*. 2002;21:1967–1977.
61. Thliveris AT, Clipson L, Sommer LL, et al. Regulated expression of Chromobox Homolog 5 revealed in tumors of ApcMin/+ ROSA11 gene trap mice. *G3 (Bethesda)*. 2012;2:569–578.
62. Robertson JD, Orrenius S, Zhivotovsky B. Review: Nucelar events in apoptosis. *J Structural Biol*. 2000;129:346–358.
63. Miller TM, Moulder KL, Knudson CM, et al. Bax deletion further orders the cell death pathway in cerebellar granule cells and suggests a caspase-independent pathway to cell death. *J Cell Biol*. 1997;139:205–217.
64. Cregan SP, MacLaurin JG, Craig CG, et al. Bax-dependent caspase 3 activation is a key determinant in p53-induced apoptosis in neurons. *J Neurosci*. 1999;19:7860–7869.
65. D'Orsi B, Bonner H, Tuffy LP, et al. Calapins are downstream effectors of Bax-dependent excitotoxic apoptosis. *J Neurosci*. 2012;32:1847–1858.
66. Zuleger N, Robson MI, Schirmer EC. The nuclear envelope as a chromatin organizer. *Nucleus*. 2011;2:339–349.
67. Babbio F, Castiglioni I, Cassina C, et al. Knock-down of methyl CpG-binding protein 2 (MeCP2) causes alterations in cell proliferation and nuclear lamins expression in mammalian cells. *BMC Cell Biology*. 2012;13:19.
68. Barnstable CJ, Dräger UC. Thy-1 antigen: a ganglion cell specific marker in the rodent retina. *Neuroscience*. 1984;11: 847–855.
69. Johnson EC, Jia L, Cepurna WO, Ackhavong V, Morrison JC. Elevated intraocular pressure affects the levels of neurofilament mRNA in the retina. *Invest Ophthalmol Vis Sci*. 2000;41:S896.
70. Chidlow G, Casson RJ, Sobrado-Calvo P, Vidal-Sanz M, Osborne NN. Measurement of retinal injury in the rat after optic nerve transection: an RT-PCR study. *Mol Vis*. 2005;11:387–396.
71. Krueger-Naug AM, Emsley JG, Myers TL, Currie RW, Clarke DB. Injury to retinal ganglion cells induces expression of the small heat shock protein Hsp27 in the rat visual system. *Neuroscience*. 2002;110:653–665.
72. Näpänkangas U, Lindqvist N, Lindholm D, Hallböök F. Rat retinal ganglion cells upregulate the pro-apoptotic BH3-only protein Bim after optic nerve transection. *Mol Brain Res*. 2003;120:30–37.
73. McKernan DP, Cotter TG. A critical role for Bim in retinal ganglion cell death. *J Neurochem*. 2007;102:922–930.
74. Leon S, Yin Y, Nguyen J, Irwin N, Benowitz LI. Lens injury stimulates axon regeneration in the mature rat optic nerve. *J Neurosci*. 2000;20:4615–4626.
75. Kitazumi I, Tsukahara M. Regulation of DNA fragmentation: the role of caspases and phosphorylation. *FEBS J*. 2011;278: 427–441.